$^{14}N(p,p')^{14}N$ reaction between 25 and 40 MeV and the tensor part of the effective interaction

S. H. Fox*
Cyclotron Laboratory and Physics Department, Michigan State University, East Lansing, Michigan 48824

Sam M. Austin
Cyclotron Laboratory and Physics Department, Michigan State University, East Lansing, Michigan 48824 and Sektion Physik, Universität München, D-8046 Garching, West Germany

(Received 30 August 1979)

Differential cross sections for the scattering of protons from ^{14}N, leaving this nucleus in its ground, 2.31- or 3.95-MeV states, were measured at bombarding energies of 29.8, 36.6, and 40.0 MeV. In addition, cross sections for the next ten excited states with $E_x < 8.7$ MeV were obtained at 29.8 MeV. Emphasis was placed on obtaining reliable results for the transition to the weakly excited $J^\pi = 0^+$, $T = 1$ state at 2.31 MeV, which is unusually favorable for studies of the tensor part of the effective interaction. The present data for the 2.31-MeV state, together with results from the literature at $E_p = 24.8$ MeV, were analyzed using a microscopic model distorted-wave approximation; contributions from the knock-on exchange amplitude and from central, tensor, and spin-orbit two-body forces were included. The fits obtained were satisfactory at 24.8 and 29.8 MeV, but failed to reproduce a peak in the cross section which appeared near 80° at the higher bombarding energies. Strengths of the tensor force were extracted and were found to be 20–75% larger than estimates based on the one-pion-exchange potential. Available evidence on the strength of the tensor force is summarized. Of the other observed states, those whose structure is dominated by $1p$-shell orbitals [at 3.95 MeV (1^+, $T = 0$) and at 7.03 MeV (2^+, $T = 0$)] were compared with microscopic distorted-wave approximation calculations using an empirically derived central force. Cross section enhancement factors were calculated in an effective charge approximation. The resulting cross sections have roughly the correct magnitude, but the shapes are only qualitatively correct. A systematic optical model analysis was carried out to provide optical model parameters for use in the distorted-wave approximation calculations. The rate of change of the real potential with bombarding energy was found to be $dV_R/dE_p = -0.50$.

[NUCLEAR REACTIONS $^{14}N(p,p')$, $E = 29.8$, 36.6, 40.0 MeV; measured $\sigma(\theta)$. Deduced optical model parameters. Microscopic distorted-wave analysis, deduced tensor effective interaction.]

I. INTRODUCTION

A number of studies of the role played by the tensor force in nuclear reactions and structure have involved the mass-14 system. The tensor force first became associated with this system through efforts to explain the anomalous Gamow-Teller β decay of ^{14}C to ^{14}N(g.s.).[1-3] Although allowed by the selection rules ($(J^\pi = 0^+, T = 1) \rightarrow (1^+, 0)$), this decay is found experimentally[4] to be strongly suppressed, having a log ft of 9.02. For a nuclear structure model with only 1p-shell orbitals, it has been shown[3,5,6] that no central-plus-spin-orbit two body interaction can account for this inhibition, but that it can be explained[1-3] by including a tensor force.

One also expects that the two body effective interaction V_{eff} used in microscopic theories of inelastic scattering and charge exchange reactions will have a tensor component. While this component is usually overwhelmed by the stronger central parts of the interaction,[7] this should not be the case for the $^{14}N(p,p')^{14}N$ (2.31 MeV) reaction we consider here or for its isospin analogs such as the $^{14}C(p,n)^{14}N$ (g.s.) reaction. A transition between states with these quantum numbers ($0^+, 1 \rightarrow 1^+, 0$) would normally be dominated by the central force part of the transition amplitude. However, since the angular momentum transfer $L = 0$ part of this central-force amplitude, is closely proportional to the matrix element for allowed β decay between these states,[8-10] it will be suppressed for the same reason the β decay is suppressed and the tensor force should be observable. The extraction of the tensor force strength should be facilitated by the fact that the remaining $L = 2$ central force contribution will have a relatively broad shape, while the tensor force contribution will be strongly forward peaked.

There have been a number of studies of this (1^+, 0) ↔ (0^+, 1) transition: $^{14}C(p,n)^{14}N$ (g.s.),[8,9,11,12] $^{14}N(p,n)^{14}O$ (g.s.),[12,13] $^{14}N(p,p')^{14}N$ (2.31 MeV),[14-17] and $^{14}N(n,n')^{14}N$ (2.31 MeV).[18] It was usually found[11-17] that including a tensor force substantially improved the description of the data, and the extracted tensor force strengths were roughly consistent with the one-pion-exchange potential (OPEP). However, the fits obtained were often of poor quality. In addition, much of the work was at energies below 20 MeV so that one could not, on a priori grounds, exclude contributions from compound nuclear processes[15] for these light nuclei. In other cases, the angular range and/or accuracy of the data was not sufficient to stringently test the theoretical model.

The present work was undertaken to obtain accurate data on the $^{14}N(p,p')^{14}N$ reaction over an extended energy and angular range. The main results reported are angular distributions for the 0.0, 2.31 and 3.95 MeV states of ^{14}N at bombarding energies of 29.8, 36.6 and 40.0 MeV. In addition, angular distributions for the next ten excited states with $E_x < 8.7$ MeV were obtained at 29.8 MeV. The experimental method and results are described in Sections II and III. Optical model fits to the elastic scattering data are described in Section IV and a brief outline of the distorted wave approximation (DWA) is given in Section V. Microscopic DWA calculations including contributions from the knock-on exchange amplitudes and from central, tensor and spin-orbit forces were carried out for those states which are well described by 1p-shell wave functions. The emphasis was on extraction of the strength of the tensor force from the data for the 2.31 MeV state. These calculations are discussed in Section VI. Finally, in Section VII, the results

of the present experiment are compared with other information on the tensor force.

II. EXPERIMENTAL PROCEDURES

A. General

The experiments were performed using protons accelerated in the MSU sector focussed cyclotron. At 29.8 MeV most of the data were taken in a 102 cm diameter scattering chamber using gas targets and a standard ΔE–E detector telescope for particle detection and identification. The absolute normalizations for the angular distributions at the higher energies were also measured with this apparatus. Some check points at 29.8 MeV and all the data at 36.6 and 40.0 MeV were taken with an Enge split-pole spectrograph, using solid melamine targets and a solid state position sensitive detector in the spectrograph focal plane.

Particle energies were determined to 0.1% from the calibration of the beam analysis system.[19] For runs on different days, but at the same nominal beam energy, the energy was reproduced to within 0.1 MeV. Beam currents were kept below 300 nA on the melamine targets and 800 nA on the gas targets to minimize deterioration of the targets and gas cell windows. The charge was measured to an accuracy of ±2%. Scattering angles were determined within ± 0.1° and ± 0.15° for the scattering chamber and spectrograph measurements respectively. Because energy resolution requirements were not severe, rather thick targets, 1 to 3 mg/cm^2, were used to reduce the counting time for the weakly-excited 2.31 MeV state.

B. Scattering chamber measurements

The cylindrical brass gas cells had 13 μm Kapton windows epoxied in place. The gas pressure ranged from 300 to 500 torr and was measured to a precision of about ± 1 torr, either with an Hg manometer or with a calibrated aneroid gauge. Decreases in the local gas density due to beam heating had been shown [20,21] to be less than 1.5% for similar beam currents and geometry.

The subtended solid angle was defined by a slit (width ≃ 3 mm) placed 11 cm from the gas cell center and an aperature (3 mm wide by 4 mm high) placed 37 cm from the center, directly in front of the detector telescope. For backward angles, $\theta \geq 120°$, the distance to the back detector was reduced to about 27 cm, reducing the counting time by a factor of two. The corresponding peak widths at 90° due to kinematic broadening alone were about 50 keV and 80 keV FWHM, respectively.

The particles were detected with a standard ΔE–E telescope consisting of a 500 μm-thick transmission mounted silicon surface barrier ΔE detector and a 5-mm thick Si(Li) E detector. The detectors were cooled by circulating alcohol in thermal contact with dry ice. The ΔE and ΔE + E signals were digitized and fed into a Xerox Data Systems Sigma 7 computer where the protons were selected digitally [22] on a ΔE vs ΔE + E display.

Individual spectra were normalized to an elastic scattering angular distribution measured with good statistics during a single short run. The effective solid angle of the detector geometry was calculated using the formulae of Silverstein.[23] A correction of 1.7% was made in the absolute normalization for counts lost due to reactions of 30 MeV protons in the detector.[24]

C. Spectrograph measurements

The ^{14}N targets used for most of the spectrograph measurements were 1–3 mg/cm^2-thick layers of melamine ($C_3H_6N_6$) evaporated from powder onto 100 μg/cm^2 carbon foil backings. An 80 wire per cm mesh of 50 μm stainless steel wire, placed over the evaporation boat and heated along with it, prevented lumps of melamine ejected from the boat from striking the target. The targets were rotated[25] at 600 rpm about an axis 1 cm above the beam and withstood beams of 300 nA for 10 to 20 hours.

Protons were detected in a silicon surface barrier position sensitive detector, 3 cm long, 1 cm high and 300 μm thick, in the focal plane of the spectrograph. Since the particles were incident at 45°, the effective thickness was 425 μm. The efficiency and linearity of the detector were mapped as a function of position and the poorer regions of the detector were avoided. A ΔE signal proportional to the energy lost by a particle passing through the detector and a ΔEX signal, proportional to the product of ΔE and X, the position, were taken from the detector and X was obtained by digital division of ΔEX by ΔE. Particle identification was similar to that for the ΔE–E telescope except that proton selection was done on a ΔE vs X display.

Because the detector subtended an energy range of only $0.02E_p$, it was necessary to vary the magnetic field of the spectrograph to bring the proton groups corresponding to different final states onto the detector. A 5 mm-thick Si(Li) monitor detector preceded by an energy degrader and placed at an angle of 150° was used to normalize the data from state to state at one angle and from angle to angle. The detector resolution was sufficient to resolve the elastic peaks of ^{12}C and ^{14}N.

The normalization of the spectrograph data was obtained from absolute measurements of the elastic scattering cross section at angles near 55° in the lab where the cross section varies slowly with angle. The techniques were the same as for the 29.8 MeV measurements (Section II B) except that a single 5 mm thick Si(Li) counter was used for particle detection. Aluminum energy degraders (1.6 mm and 2.9 mm thick at 36.6 and 40.0 MeV respectively) slowed the protons to about 30 MeV so they stopped in the detector. A correction of about 1% was made for flux lost due to reactions in the absorbers [26,27] and particles elastically scattered out of the detector solid angle, in addition to the 1.7% correction for reactions in the detector. The overall normalization uncertainty is less than ±4%.

III. EXPERIMENTAL RESULTS

The resolution for the spectra obtained in the scattering chamber ranged from 80 keV at forward angles to almost 105 keV near 90° where kinematic broadening was larger. Elastic peak to background ratios were about 2000 to 1. A spectrum is shown in Fig. 1; all states below 8.7 MeV are visibly resolved except for the members of the 7.97–8.06 MeV doublet. The 0^+, T = 1 level at 8.62 MeV is not appreciably populated. As expected, the 2.31 MeV state is very weakly excited. The peak at an apparent E_x of 1.87 MeV arises when protons elastically scattered from ^{14}N subsequently scatter inelastically from ^{28}Si, leaving it in its 1.78 MeV 2^+ state; the deexcitation γ ray then escapes from the detector.[28–32] That this peak is somewhat broader than a normal peak and that its centroid location is shifted are presumably due to incomplete charge collection for the recoiling silicon ions.

The automatic fitting routine SAMPO [33] was used in the reduction of the data. To determine the peak shape parameters as a function of energy, the isolated peaks at 0.0, 3.95 and 7.03 were fitted with a Gaussian plus one exponential tail on either side of the peak. The program then adjusted the amplitude and centroid of two such shapes to fit the doublets at 4.92–5.11 MeV, 5.69–5.83 MeV, 7.97–8.06 MeV, and 8.49–8.62 MeV. The 8.62 MeV state was not observed and had a strength less than 10% of that of the 8.49 MeV state at all angles. An estimate of the fitting error was obtained from tests on

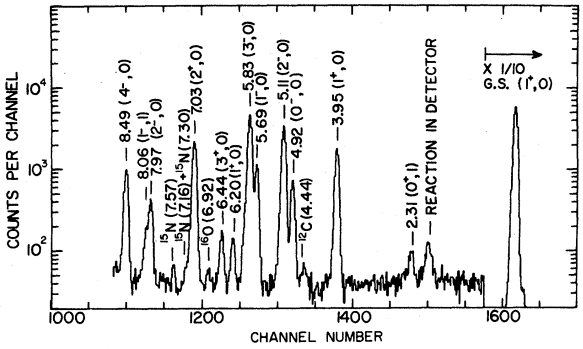

Fig. 1. Energy spectrum taken with the detector telescope at E_p = 29.8 MeV, θ_{lab} = 50°. The energy level parameters are taken from Ref. 4. The peak labeled "Reaction in Detector" arises from interactions of elastically scattered protons with ^{28}Si in the detector as discussed in the text. Other small impurity peaks are also noted. The energy resolution is 80 keV, FWHM.

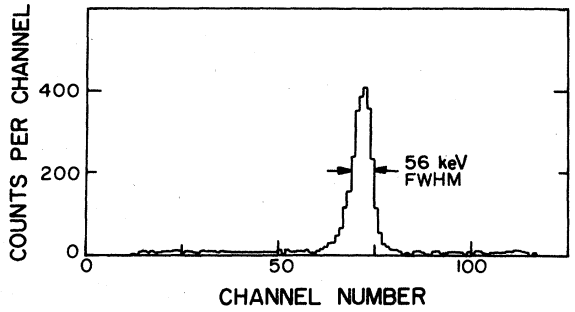

Fig. 2. Energy spectrum in the neighborhood of the 2.31 MeV peak, taken with the spectrograph at E_p = 40 MeV, θ_{lab} = 70°. The energy resolution is 56 keV, FWHM.

artificially synthesized doublets of known intensity and separation. Background subtraction errors were estimated by obtaining peak intensities for high and low estimates of the background.

Table I. Differential cross sections (μb/sr) for the $^{14}N(p,p')^{14}N$ (2.31 MeV) reaction at 24.8, 29.8, 36.6, and 40.0 MeV. Angles are measured in degrees.

24.8 MeV[a]		29.8 MeV[b]		36.6 MeV[b]		40.0 MeV[b]	
$\theta_{c.m.}$	$\frac{d\sigma}{d\Omega}\Big\|_{c.m.}$	$\theta_{c.m.}$	$\frac{d\sigma}{d\Omega}\Big\|_{c.m.}$	$\theta_{c.m.}$	$\frac{d\sigma}{d\Omega}\Big\|_{c.m.}$	$\theta_{c.m.}$	$\frac{d\sigma}{d\Omega}\Big\|_{c.m.}$
20.4	360 (42)	10.7	204 (5)	10.7	112 (5)	10.7	120 (5)
21.4	215 (16)	21.4	137 (5)	12.9	123 (8)	18.2	104 (5)
26.8	145 (14)	21.5	187 (8)	18.2	104 (8)	21.5	101 (5)
32.1	118 (17)	26.8	107 (5)	21.5	88 (5)	26.8	76 (5)
36.4	90 (11)	32.1	81 (5)	26.8	76 (5)	32.1	54 (5)
41.7	78 (15)	37.4	55 (5)	32.1	56 (5)	37.4	33 (5)
48.0	48 (8)	42.7	38 (5)	37.4	30.0(5)	42.7	16.5(5)
52.3	44 (14)	48.0	25.0(5)	42.7	18.5(5)	48.0	8.0(5)
58.5	28.5(11)	53.2	19.0(5)	48.0	8.9(5)	53.3	7.7(5)
63.8	22.5(13)	58.5	16.5(5)	53.3	7.1(5)	58.5	11.0(5)
74.1	21.0(14)	63.7	15.5(5)	58.5	9.1(5)	63.7	16.5(5)
83.3	24.8(11)	68.8	16.0(5)	63.7	13.0(5)	68.9	21.5(5)
93.4	27.3(12)	74.0	19.5(5)	68.8	18.0(5)	74.0	24.0(5)
104.3	22.8(12)	79.2	21.5(9)	74.0	19.0(8)	79.1	23.5(5)
114.2	27.0(9)	84.1	22.0(5)	79.1	20.5(5)	84.2	23.0(5)
123.8	31.2(6)	89.4	23.0(9)	84.2	18.0(8)	89.2	18.0(5)
133.4	28.8(8)	94.2	22.5(5)	89.2	17.0(8)	94.3	15.0(5)
142.8	22.0(8)	99.4	23.5(9)	94.2	13.5(5)	99.2	10.0(5)
152.2	20.7(8)	104.3	23.0(9)	99.2	10.5(8)	104.2	7.5(6)
161.5	23.4(6)	109.1	19.0(5)	104.2	7.8(8)	114.0	4.7(6)
		114.1	18.0(8)	109.1	7.2(5)	123.7	4.3(6)
		119.0	19.0(8)	114.0	6.1(8)		
		123.8	16.0(5)	118.8	6.3(8)		
		128.6	14.0(8)	123.7	6.1(6)		
		133.4	9.8(8)	128.5	4.8(10)		
		138.1	6.5(8)	138.0	3.3(18)		
		142.8	5.9(12)				
		147.5	6.6(8)				
		152.2	9.5(8)				
		156.9	16.0(8)				
		162.4	28.0(8)				
		166.1	30.5(8)				

[a] From Ref. 17.

[b] The quantity in parentheses is the relative error in percent. The normalization error of about 4% is not included.

[c] The results at 29.8 MeV are the average of the data taken in the spectrograph and in the scattering chamber.

The 2.31 MeV peak was given special attention. At forward angles when the Si reaction peak was clearly separated from it, both states were treated as singlets. The average value of the ratio of the counts in the silicon peak to those in the elastic peak was $(20 \pm 2) \times 10^{-4}$ for elastically scattered protons with energies ranging from 29.5 MeV (at 20°) to 26 MeV (at 85°).

At back angles kinematic shifts moved the peaks sufficiently close so they were not cleanly separated. Fortunately the Si peak is small at these angles because the elastic scattering cross section is relatively small. In this case two methods were used to extract the 2.31 MeV intensity. In one the Si peak and the 2.31 MeV peak were treated as a doublet and SAMPO was used to extract the intensity of the 2.31 MeV state. Another measure of the intensity was obtained by subtracting $(20 \times 10^{-4}) \times$ (elastic peak yield) from the total number of counts above background in the combined Si + 2.31 MeV peaks. Between 90° and 165° the elastic protons have energies beween 26 and 22 MeV and the 20×10^{-4} factor is in good agreement with the available data.[28-32] The cross section was taken to be the average of these two estimates and the error one third the difference.

The analysis of the spectrograph data was much more straightforward. The spectrum shown in Fig. 2 has a peak to background ratio of about 50 to 1 and the ratio remained above 8 to 1 even at the most forward angles.

The resulting angular distributions are shown in Figs. 3–6 and Table I, along with the angular distribution for the 2.31 MeV state measured by Crawley et al.[17] at

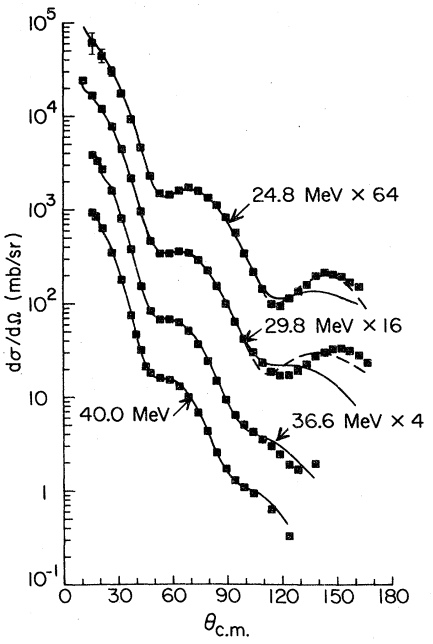

Fig. 3. Differential cross sections for elastic scattering. Where not shown the relative errors are smaller than the points and are typically 3% at the forward angles and 4% at the backward angles. The data at 24.8 MeV is from Ref. 17. The cross sections have been multiplied by the factor shown for display purposes. The curves are the results of optical model fits using the parameters of Table II. The solid curves are for the standard optical model ($r_{SO} = r_R$, $a_{SO} = a_R$) and the dashed curves for the optical model with a modified spin-orbit well and free spin-orbit parameters.

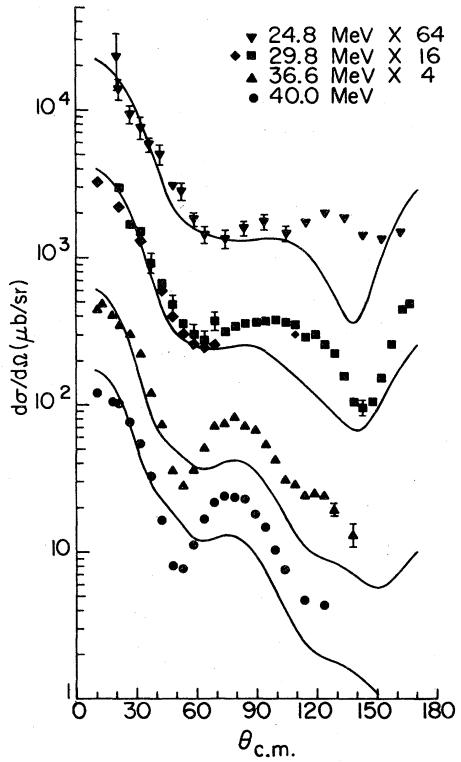

Fig. 4. Differential cross sections for inelastic scattering to the 2.31 MeV state. At 29.8 MeV the points (◆) were taken in the spectrograph and the points (■) were taken in the scattering chamber. The data at 24.8 MeV are from Ref. 17. The cross sections have been multiplied by the factor shown for display purposes. The curves are the final theoretical fits obtained as described in Sec. VI D and are calculated from the force $\sqrt{f}$ (S + 1.25 × OPEP + LS), where the factor f is given in Table VI.

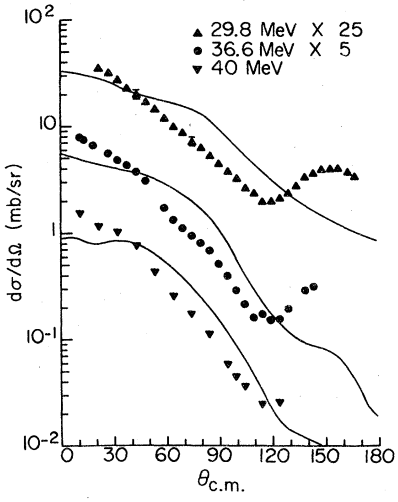

Fig. 5. Differential cross sections for inelastic scattering to the 3.95 MeV state. The cross sections have been multiplied by the factor shown for display purposes. The curves are calculated using the SMA force and an effective charge approximation as described in Sec. VI E.

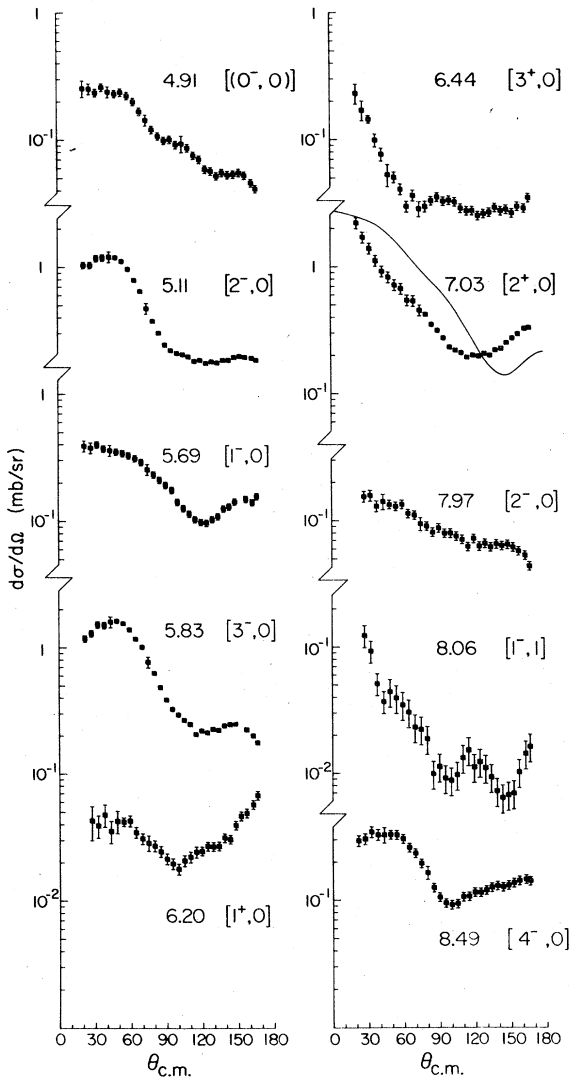

Fig. 6. Differential cross sections for inelastic scattering to states with $E_x > 4$ MeV at $E_p = 29.8$ MeV. The theoretical curve for the 7.03 MeV state is calculated as described in Sec. VIE.

24.8 MeV. The errors shown include statistics, uncertainties in background subtraction and the peak fitting uncertainties, but not the 4% uncertainty in the normalization. At 29.8 MeV an error due to nonreproducibility of angles in the normalization run is also included.

All of the states which are strongly excited (3.95, 5.11, 5.83, and 7.03 MeV) can be reached by non-spin-flip transitions with L = 2 or 3. The 6.20 state also is fed by such amplitudes, but is very weakly excited with maximum cross section of less than 100 μb/sr. The relative excitation strengths are in good general agreement with the results of (p,p') experiments at 10.6 MeV to 14.6 MeV,[14,15] except that the cross section for the 6.20 state is much larger at these energies. In addition, Curtis et al.[15] find that the 8.62 MeV state has a substantial cross section for $\theta < 40°$, inconsistent with our results.

The angular distribution of Crawley et al.[17] at 24.8 MeV differs from those at higher energies in that it has no dip at backward angles. There is, however, some evidence for a resonance contribution to the 24.8 MeV cross section in the data of Lutz et al.[15] These authors have measured excitation functions for $^{14}N(p,p')^{14}N$ (2.31 MeV) at $\theta_{c.m.} = 90°$, 125°, and 160°. Although the authors state[15] that there is no evidence of resonance behavior for 17 MeV $< E_p <$ 26.5 MeV, the data for 125° (presented in Fig. 2 of Lutz et al.[15]) have a peak about 15 μb/sr high near 25 MeV. There is no evidence for similar structure at 90° and 160°. A compound nucleus contribution of 15 μb/sr would account for about half the cross section we observed at 125°; thus the part of the cross section attributable to a direct reaction might indeed have a mild dip at 125°, rather than the peak seen in the measured cross section.

IV. OPTICAL MODEL ANALYSIS

A. Standard optical model

An optical model analysis of the elastic scattering data at 24.8,[17] 29.8, 36.6 and 40.0 MeV was made to obtain optical model parameters for use in the DWA calculations. In an attempt to find parameters which varied smoothly with energy, an average set of geometrical parameters was determined which fit all the data reasonably well. The potential strengths were then varied to fit the data at each energy.

Most of the optical model searches were done with the code GIBELUMP.[34] The potential employed had the form

$$V_{opt}(r) = V_C(r) - V_R f(x_R) - i\,(W_S - 4W_D \frac{d}{dx_I}) f(x_I) + V_{SO} (\frac{\hbar}{m_\pi c})^2 \frac{1}{r} \frac{d}{dr} f(x_{SO})\, (\vec{l}\cdot\vec{\sigma}), \quad (1)$$

where

$$f(x) = (1 + e^{x_i})^{-1}, \qquad x_i = \frac{r - r_i A^{1/3}}{a_i},$$

and V_C is the Coulomb potential of a uniformly charged sphere of radius $R_C = r_c A^{1/3}$.

During preliminary searches it was found, as is often the case with light nuclei,[35,36] that no reasonable potentials could accurately reproduce the data beyond the second minimum in the cross section near 105°. To prevent these points from unduly influencing the search and the extracted parameters, the errors on these points were about doubled (tripled for the 29.8 MeV data). Allowing the spin-orbit geometry parameters r_{SO} and a_{SO} to vary led to somewhat improved fits at backward angles at 24.8 and 29.8 MeV, but the parameters tended to values that were rather large in the case of r_{SO}($r_{SO} \gtrsim 1.35$ fm) and small in the case of a_{SO}($a_{SO} \lesssim 0.45$ fm). Because the two-body spin-orbit force has a short range it seems unreasonable to have $r_{SO} > r_R$. Since the fits beyond the second minimum were not precise in any case and since polarization data are needed to convincingly determine the spin-orbit well, the spin-orbit geometrical parameters were set equal to those of the real potential in the searches directed at finding an average geometry.

With the restrictions $r_{SO}=r_R$, $a_{SO}=a_R$, searches were performed using as starting parameters six different sets of parameters obtained by others in this mass and energy range.[35-40] An energy independent set of geometrical parameters was then chosen which provided the best compromise fit at all energies and the data were refitted allowing only the potential strengths to vary. The final parameters are shown in Table II. The fits were most sensitive to changes in r_R, V_R, and r_I. We did not search

Table II. Optical model parameters for $^{14}N + p$.

E_p (MeV)	24.8		29.8		36.6	40.0
	Average Geometry[a]	Modified Spin Orbit[b]	Average Geometry[a]	Modified Spin Orbit[b]	Average Geometry[a]	Average Geometry[a]
V_R (MeV)	51.4	52.4	49.1	49.3	45.7	43.8
r_R (fm)	1.133	1.133	1.133	1.133	1.133	1.133
a_R (fm)	0.651	0.651	0.651	0.651	0.651	0.651
W_S (MeV)	1.56	1.53	2.93	2.93	5.76	5.75
W_D (MeV)	4.75	4.69	3.52	3.63	1.63	1.93
r_I (fm)	1.345	1.345	1.345	1.345	1.345	1.345
a_I (fm)	0.509	0.509	0.509	0.509	0.509	0.509
V_{SO} (MeV)	4.24	3.91	5.31	5.08	5.60	8.61
r_{SO} (fm)	r_R	1.30	r_R	1.33	r_R	r_R
a_{SO} (fm)	a_R	0.394	a_R	0.350	a_R	a_R
r_C (fm)	1.25	1.25	1.25	1.25	1.25	1.25
χ^2/N[c]	31	6.4	100	35	4.5	3.2

[a] For the average geometry described in Section IV A.

[b] For the modified spin-orbit geometry described in Section IV B.

[c] Value of χ^2 is calculated for the actual errors on the experimental data, not for those used in the search (see Section IVA). N is the number of degrees of freedom in the search.

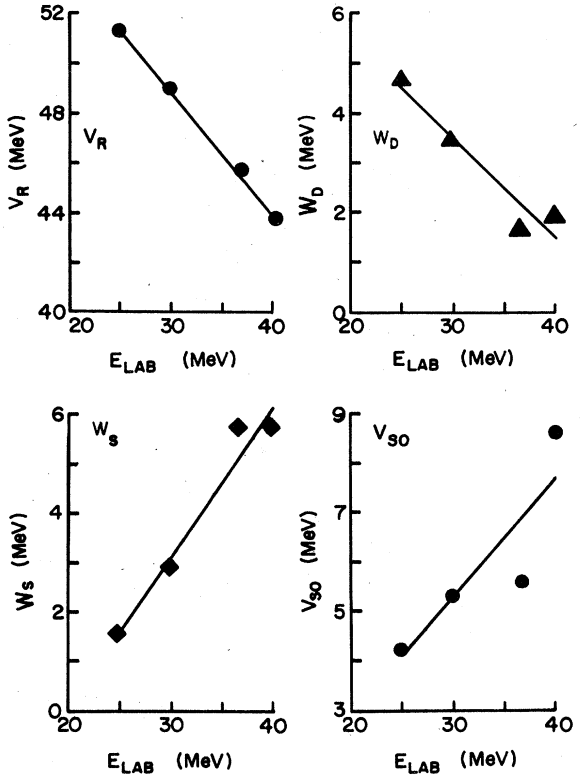

Fig. 7. Potential strengths for the standard optical model as a function of E_p. The solid lines are the linear fits of Eq. (2).

on the overall normalization, but small changes of the normalization did not significantly change the resultant χ^2. Cross sections calculated with these parameters are shown in Fig. 3. As is obvious from this figure, the large values of χ^2 at 24.8 and 29.8 arise from the poor fit to the large angle data.

In Fig. 7 the potential strengths are plotted as a function of bombarding energy. The variation of the potential strengths with bombarding energy is given approximately by the following linear relationships

$$V_R = 63.8 - 0.50\,E_p, \qquad W_D = 9.7 - 0.204\,E_p,$$
$$W_S = -5.9 + 0.30\,E_p, \qquad V_{SO} = -1.9 + 0.24\,E_p, \tag{2}$$

where the potential strengths and laboratory bombarding energy are expressed in MeV. These relationships are valid between 24 and 40 MeV and were obtained by unweighted linear least squares fits to the parameters of Table III. This slope of V_R with respect to E_p is similar to the value of −0.55 found by Perey[41] (fitting ^{27}Al to ^{197}Au) but is substantially larger than the values of −0.22 to −0.32 usually obtained[42,43] for medium and heavy nuclei in this energy range. Van Oers and Cameron[36] have summarized available information on $p + {}^{16}O$ elastic scattering in the energy range from 0 to 53 MeV. The slope obtained from a straight line fit over the entire energy range is −0.56 in good agreement with our result. However, while the points between 23 and 53 MeV are probably consistent with this value within the uncertainty of the analysis, they are better fitted by a slope of −0.29.

B. Modified spin-orbit form factor

Although the usual Thomas expression (Eq. 1) for the spin-orbit potential has a 1/r singularity at the origin, for medium and heavy nuclei the potential has a basically

Table III. The central part of the effective interaction.

Potential	S[a]	HJ_4[b]	HJ[c]	G[d]	BJ[e]	SMA[f]
V_{00} (MeV)	-10.41	24.8	-29.5	+4.82	-16.85	-28.0
μ_{00} (fm)	1.415	1.06	1.00	1.00	1.359	1.00
V_{01} (MeV)	3.47	12.8	12.1	-4.82	7.28	11.0
μ_{01} (fm)	1.415	0.98	1.00	1.00	1.359	1.00
V_{10} (MeV)	3.47	4.6	7.6	-4.82	3.95	11.0
μ_{10} (fm)	1.415	1.18	1.00	1.00	1.359	1.00
V_{11} (MeV)	3.47	8.3	9.8	+4.82	5.62	11.0
μ_{11} (fm)	1.415	1.06	1.00	1.00	1.359	1.00
σ_T (mb)[g]	0.21		0.48	0.22[h]	0.49	0.54

[a] Ref. 13. From a fit of a Serber force with a range of 1.415 fm to the small momentum components of the long range part of the Hamada-Johnston potential.

[b] Ref. 45. From matching J_0 and J_2 to the long range part of the Hamada-Johnston potential.

[c] Ref. 45. From matching J_0 for a Yukawa with a range of 1.0 fm to the long range part of the Hamada Johnston potential.

[d] Ref. 67. An odd state force obtained by fitting the 1p phase shifts. Always used in conjunction with interaction HJ and labeled HJ + G.

[e] Ref. 68. From a fit to the low energy scattering data.

[f] Ref. 7. V_{00} and V_{11} were determined from a survey of inelastic scattering analyses. V_{01} and V_{10} were set equal to V_{11}.

[g] Evaluated at E_p = 29.8 MeV, direct plus exchange.

[h] Calculated for HJ + G.

surface peaked shape. However, in a nucleus as light as ^{14}N where $df(x_{SO})/dr$ remains large near the origin, this is no longer true.[39] It seemed possible that the tendency of the search program to make r_{SO} large and a_{SO} small was an attempt to reduce $df(X_{SO})/dr$ near the origin and hence to reduce the contribution from the nuclear interior.

To investigate this possibility we used a modified spin-orbit potential introduced by Watson et al.[39] in their analysis of elastic scattering from 1p shell nuclei:

$$V_{SO}(r) = V_{SO}\left(\frac{\hbar}{m_\pi c}\right)^2 \frac{1}{r_{SO}A^{1/3}} \frac{df(x_{SO})}{dr} . \quad (3)$$

I.e. the factor 1/r in the Thomas expression is replaced by (nuclear radius)$^{-1}$, a constant.

The 24.8 and 29.8 MeV data were fitted using the average geometry found in Section IV A for the real and imaginary wells, but allowing r_{SO}, a_{SO} and the potential strengths to vary. The results are shown in Table II and Fig. 3. The spin orbit well radius again tends to large values, $r_{SO} > r_R$ and the fits are only slightly improved over fits with Eq. (1) and free spin-orbit geometrical parameters. It appears that the singularity in the shape of the spin orbit potential is not solely responsible for the back-angle discrepancy.

V. OUTLINE OF DWA THEORY

In the distorted wave approximation (DWA), neglecting the knock-on exchange amplitude, the cross section for an inelastic scattering reaction is proportional to the square of the transition amplitude [44]

$$T_{fi} = \int \chi_f^{(-)*} \langle \psi_f | V_{eff} | \psi_i \rangle \chi_i^{(+)} d\vec{r} ,$$

where $\chi_i^{(+)}$ and $\chi_f^{(-)}$ are the incoming and outgoing distorted waves and ψ_i and ψ_f are the initial and final target states. Assuming that V_{eff} can be written as the sum of the two-body interactions V_{ip} between the projectile p and the target nucleons i, one has

$$V_{eff} = \sum_i V_{ip} ,$$

the sum being over the valence target nucleons. The central part of V_{ip} can be written as

$$V_{ip}^{cent}(r) = V_{00}(r) + V_{10}(r)\vec{\sigma}_i \cdot \vec{\sigma}_p + V_{01}(r)\vec{\tau}_i \cdot \vec{\tau}_p + V_{11}(r)(\vec{\sigma}_i \cdot \vec{\sigma}_p)(\vec{\tau}_i \cdot \vec{\tau}_p) , \quad (4)$$

where the subscripts on the V_{ST} are the spin S and isospin

T transferred in the reaction.

For the transition of most interest here, $^{14}N(p,p')^{14}N$ (2.31 MeV), one has $(J = 1^+, T = 0) \rightarrow (0^+, 1)$. The selection rules for the direct process then allow only the amplitudes with (L,S,J,T) = (0,1,1,1) or (2,1,1,1) where L,J are the transferred orbital and total angular momentum. Thus only $V_{\sigma\tau}$ can contribute to the reaction. The (0,1,1,1) amplitude for inelastic scattering is closely proportional to the matrix element for the Gamow-Teller β decay of ^{14}C.[8-10] Since this decay is strongly inhibited, the normally dominant L = 0 contribution to the cross section is suppressed and the (2,1,1,1) amplitude is dominant.

If a tensor force is added to V_{ip} the selection rules are somewhat relaxed. For the tensor force amplitudes,[11,13]

$$S = 1,$$

$$L = \lambda, \lambda \pm 2,$$

where $\vec{L}$ and $\vec{\lambda}$ are the orbital angular momenta transferred to the projectile and target respectively (for central forces $\lambda = L$). The $\lambda = L = 0$ amplitude is suppressed just as is the L = 0 amplitude for a central force. But the $\lambda = 2$, L = 0 amplitude need not be small and in fact turns out to be a comparable to the $\lambda = L = 2$ amplitude for the central force.

When the formalism is modified[45-48] to include the effects of knock-on exchange the selection rules are again relaxed. For central forces the angular momenta transferred need not satisfy the $\Delta\pi = (-1)^L$ condition,[45] but in cases studied to date the amplitudes for these non-normal parity L transfers are unimportant[49] for small L transfers. The selection rules that govern the tensor exchange amplitudes are quite complex and are found, for example, in Ref. 50. $\Delta\pi$ need be neither $(-1)^L$ or $(-1)^\lambda$, and non-normal L transfers are also allowed.

VI. MICROSCOPIC MODEL CALCULATIONS

The microscopic model calculations were done with the code DWBA 70[51] which permits one to include the contribution of the knock-on exchange amplitude and central, tensor and spin-orbit terms in the effective interaction. One then has

$$V_{ip} = V_{ip}^{coul} + V_{ip}^{cent} + (V^{LS} + V_\tau^{LS}\vec{\tau}_i \cdot \vec{\tau}_p)\vec{L}\cdot\vec{S} + (V^{ten} + V_\tau^{ten}\vec{\tau}_i \cdot \vec{\tau}_p)r^2 S_{ip}, \quad (5)$$

where V^{coul} is the Coulomb interaction, V^{cent} is the central interaction given in Eq. (4), and S_{ip} is the usual tensor operator. Since S = 1 for tensor and spin orbit forces, we simply indicate by the symbol τ when T = 1. Except for V^{coul} all the V's occuring in Eqs. 4 and 5 were constrained by the code to have a Yukawan dependence on the interparticle distance r with a range μ, namely,

$$V(r) = V\frac{e^{-r/\mu}}{r/\mu}.$$

The radial form of the tensor force is then $r^2 \times$ Yukawa.

A. Optical model potentials

The parameters of the optical potentials for the incident channel were obtained from Table II. For the exit channel energy $E_{p'}$, the parameters were obtained by linear interpolation between the measured points. $E_{p'}$ was given by

$$E_{p'} = E(\text{incident}) - \frac{15}{14}E_x,$$

where E_x is the excitation energy of the level involved. To assess the sensitivity of the calculations to the optical model potentials another set of optical model parameters was found. The geometry was that used by Crawley et al.[17] at 24.8 MeV ($r_R = r_I = r_{SO} = 1.20$ fm, $a_R = a_{SO} = 0.57$ fm, and $a_I = 0.60$ fm) and the potential strengths were varied to fit the elastic scattering data as in Section IV. Although this geometry was quite different from that found here, it fit the elastic scattering data quite well, especially at 24.8 and 29.8 MeV, and made little difference in the calculated inelastic scattering cross sections (see Fig. 8).

B. Wave functions

The wave functions used in most of the calculations were from Cohen and Kurath (CK),[52] and assume a closed ^{4}He core with ten particles (or two holes) in the 1p shell. The CK wave functions contain the dominant components[53] of the 0.0, 2.31, 3.95 and 7.03 states in ^{14}N and strongly suppress the β decay of ^{14}C, predicting log ft = 5.42. Although much less than the experimental value of 9.02,[4] this is still a strong suppression as one can see[52] by comparison with simple calculations or with the ft value of 2.91 for the somewhat analogous decay of ^{6}He.[54] Consequently the CK wave functions predict a small $L = \lambda = 0$ inelastic scattering amplitude. States of ^{14}N other than those noted above contain important components of 2s-1d shell orbitals[53,55,56] and were not treated here.

The wave functions were obtained using the Oak Ridge-Rochester[57] shell model code, the two-body matrix elements ((8-16)2BME) and single particle energies found by CK[52] in a fit to levels in nuclei with masses 8-16. From these wave functions, the necessary spectroscopic amplitudes[44,51] were generated with the code MULTISCAT.[58] Harmonic oscillator radial wave functions were used, with the oscillator parameter a = 1.68 fm obtained from electron scattering data.[59,60]

Several calculations were made to check the sensitivity of the calculations to parameter choices. Shown in Fig. 8 are the results for radial wave functions generated in a Saxon-Woods potential and for different values of the oscillator constant. The cross sections are insensitive to reasonable variations of these parameters. Results for different wave functions are shown in Fig. 9. Wave functions calculated from Cohen Kurath (8-16) POT two body matrix elements yield cross sections very similar to those calculated from (8-16)2BME matrix elements. Some calculations were also done with spectroscopic amplitudes derived from electron scattering data.[61] These amplitudes yield rather different results.

C. Effective interactions

In a nucleus as light as ^{14}N, inelastic scattering data are often not described accurately by DWA calculations and it is easy to be led astray if one allows himself complete freedom in the choice of fitting parameters. Thus, it was felt desirable to have an a priori estimate of V_{eff} so that fits could be made by relatively small adjustments of strength parameters. There are several difficulties in obtaining such estimates. Although a number of central interactions have been used, they are not all consistent[62] and there is very little information[7,63-65] on the tensor and spin-orbit forces. In addition, many of the available interactions do not have the Yukawan radial dependence required by the code DWBA 70. Where necessary we have obtained the range and strength of the equivalent Yukawa interaction by matching the first two terms in the expansion of the Fourier transform of the interaction. For the central force these terms are proportional to the volume and r^2

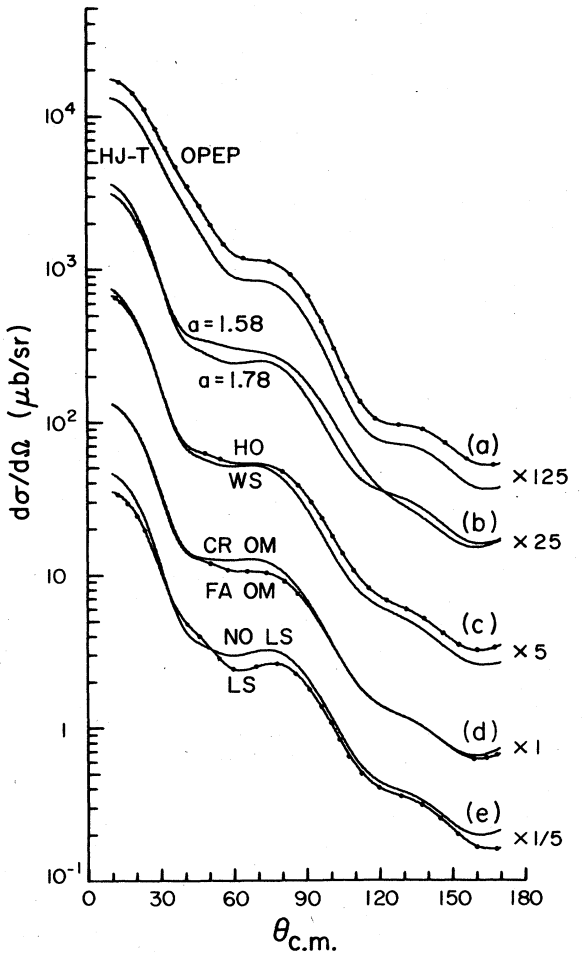

Fig. 8. Effects of parameter choices and approximations on cross sections for the 2.31 MeV state at 40 MeV. Except as noted the calculations are with the usual parameters and a force S + OPEP. (a) Calculated using only a tensor force with parameters from Table V. The HJ-T force is for R_{co} = 0.49 fm. (b) Calculated for the harmonic oscillator parameters a = 1.58 fm and a = 1.78 fm. (c) Calculated with harmonic oscillator radial wave functions with a = 1.68 (labeled HO) and for radial wave functions generated in a Woods-Saxon potential (WS). The WS potential depth was fixed to give the single particle energies labeled (8–16) 2BME in Ref. 52. (d) Calculated for the optical model parameters of Table III (FA OM) and for parameters derived from the geometry of Ref. 17 as described in Sec. VI A (CR OM). (e) Calculated with the S + 1.25 × OPEP + LS force (LS) and with the S + 1.25 × OPEP force (NO LS). The cross sections have been multiplied by the factor shown for display purposes.

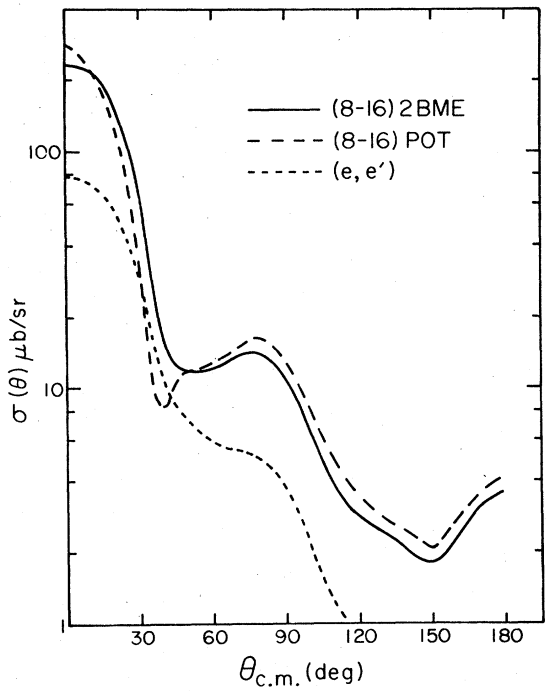

Fig. 9. Differential cross sections for exciting the 2.31 MeV state as calculated at E_p = 36.6 MeV with S + 1.25 × OPEP forces and the wave functions labeled (8–16) 2BME and (8–16) POT from Ref. 52, and (e,e') from ref. 61.

weighted integrals of the interaction, or in other words to J_0 and J_2 where

$$J_n \equiv 4\pi \int_{R_{co}}^{\infty} r^n V(r) r^2 dr.$$

In the cases of the tensor and spin orbit forces these terms are proportional to J_2 and J_4.[63,66]

From the available central interactions we have chosen the set shown in Table III. The force labeled SMA was obtained from a survey of inelastic scattering analysis,[7,64] and the remainder from analyses of nucleon-nucleon scattering data.

Two estimates of the tensor interaction were made, one based on the one-pion-exchange potential (OPEP) and the other on the Hamada-Johnston[69] tensor potential (HJ-T). The parameters of the equivalent (r^2 × Yukawa) interactions needed for DWBA 70 were obtained by matching J_2 and J_4 integrals as outlined above, where R_{co} was 0 for OPEP and was varied from 0.49 fm (approximately the hard core radius) to 1.0 fm for HJ-T. The results shown in Table IV are essentially independent of R_{co}. In the case of OPEP, V^{ten} is identically zero, and this quantity is also small for HJ-T, so, at least in the direct amplitude, the tensor force contributes in an important way only to isospin transfer T = 1 cross sections. In preliminary calculations the OPEP and HJ-T forces were found to yield cross sections essentially identical in shape and differing in magnitude by about 30% as shown in Fig. 8. In all other work described here we use a force with the shape of the OPEP force of Table IV, but with adjustments in strength to improve the fit to the data.

Spin-orbit forces were also derived from the Hamada-Johnston[69] potential for several values of R_{co}. In contrast to the tensor force the strength of the spin-orbit force shown in Table V is extremely sensitive to R_{co}, increasing as R_{co} decreases. Its strength for R_{co} = 0.49 fm, as measured by $J_2/4\pi$ = -34.9 MeV fm,[5] is similar to those used in previous work on inelastic scattering,[63] but is about half the value of 80 MeV fm[5] implied (ignoring exchange) by the usual optical model spin orbit potentials.[70] It is not clear whether exchange

Table IV. The tensor part of the effective interaction.

Source	V_T^{ten} (MeV fm^{-2})	μ (fm)	J_2 (MeV fm^5)
OPEP	11.01	0.816	4000
HJ-T[a] (R_{co} = 1.0 fm)	7.07	0.857	3620
(R_{co} = 0.6 fm)	7.64	0.850	3690
(R_{co} = 0.49 fm)	7.74	0.849	3710
BBML[b]			2260
BBML[c]			2833

[a] R. Schaeffer and S.M. Austin, unpublished.

[b] Interactions labeled 11 and 14 in Table I of Ref. 11.

[c] Interactions labeled 9 and 14 in Table I of Ref. 11.

effects in the microscopic calculation of the optical model spin orbit potential can remove this discrepancy. In the calculations reported here we use the values for R_{co} = 0.49 fm, denoting this force by LS. The contributions of the spin-orbit force are found to interfere destructively with the other amplitudes, decreasing the cross section by about 15% without appreciably changing its shape (see Fig. 8).

The data were also compared (see Fig. 10) with the predictions of an interaction derived by Bertsch et al.[62,65] by fitting shell model G matrix elements. This interaction is the sum of three Yukawas with the ranges chosen to reflect various meson exchanges. Central, tensor and spin-orbit components were included.

In the discussion which follows we refer to the various pieces of V_{eff} by the identifying initials from Tables III-V. Thus, for example, S + 1.25 × OPEP + LS means the central interaction labeled S from Table III, plus a tensor interaction with 1.25 times the strength of the potential labeled OPEP in Table IV plus the spin orbit interaction LS from Table V.

D. Results and discussion-2.31 MeV state

The results of calculations including central or tensor forces by themselves are shown in Fig. 11. As expected, central forces alone cannot account for the data; the calculated cross sections have a broad, unstructured L = 2 shape with too gentle a slope at forward angles. Tensor forces alone describe the data at small angles fairly well, but the predicted cross sections beyond the first minimum are too small. While the contribution of the knock-on exchange amplitude does not substantially affect the shape of the angular distributions in either case, exchange

Table V. The spin orbit part of the effective interaction.

Determination	$J_2(T=0)/4\pi$ (MeV fm^5)	$J_2(T=1)/4\pi$ (MeV fm^5)	$V^{LS}_{T=0}$ (MeV)	$V^{LS}_{T=1}$ (MeV)	μ_{LS} (fm)
Optical Model[a]	-80				
HJ(R_{co} = 1.0 fm)[b]	- 7.3	- 6.5			
HJ(R_{co} = 0.6 fm)	-27.7	-13.7			
HJ(R_{co} = 0.49 fm)[c]	-34.9	-16.2	98.4	18.0	0.557
			-4496	-1488	0.301

[a] Ref. 70.

[b] From the part of the Hamada-Johnston potential with $r \geq R_{co}$.

[c] The potential is the sum two terms, one with a range of 0.557 fm, the other with a range of 0.301 fm. This potential is referred to in the text as LS.

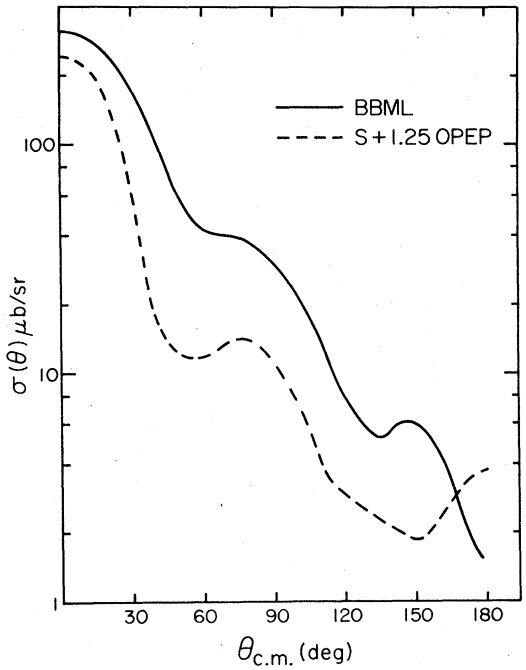

Fig. 10. Differential cross sections for exciting the 2.31 MeV state as calculated at 36.6 MeV with (8–16) 2BME wave functions. The curves are for the force S + 1.25 × OPEP and the G matrix force of Ref. 26 (BBML).

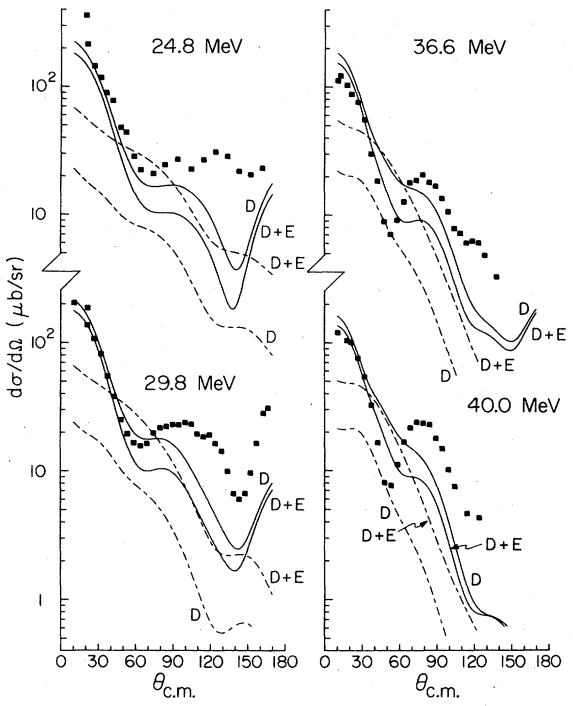

Fig. 11. Differential cross sections for exciting the 2.31 MeV state calculated with S central forces alone (dashed curves) or with OPEP tensor forces alone (solid curves). The curves labeled D are for the direct amplitude only, while those labeled D + E include both the direct and exchange amplitudes. The data points are identical to those of Fig. 4, except that at 29.8 MeV the results of separate measurements in the scattering chamber and spectrograph have been combined.

increases the cross section for central forces and decreases that for tensor forces. As a result, the direct (D) and direct-plus-exchange (D + E) cross sections calculated with a combination of central and tensor forces differ in shape as well as in magnitude. The D cross section tends to have a highly structured shape, dominated by the tensor amplitude, while in the D + E cross section, the tensor amplitude will be reduced and the central amplitude increased, resulting in a less structured angular distribution, more nearly resembling that for the central force.

Calculations were performed for each of the central forces in Table III. The HJ–T tensor force (see Table IV) was used with the HJ and HJ + G forces and the OPEP tensor force with the other central forces. To conserve computer time, no spin-orbit force was included at this point, as it had been shown that substantial modifications in shape were unlikely. The results were disappointing. Cross sections calculated with strong central forces (as measured by the total cross section for V^{cent} alone – see Table III) are reasonable in magnitude, but the shapes are structureless and too much like those for a pure central force. Results for the HJ central + HJ–T force are shown in Fig. 12; those for SMA + OPEP are quite similar. On the other hand, calculations with weak central forces (e.g. S or HJ + G) give more acceptable shapes, with the best results for S + OPEP, but the cross sections are too small by about a factor of two (see Fig. 12). Calculations with the BJ force, which has an exchange mixture and strength similar to the HJ force, but a range of 1.36 fm rather than 1.00 fm, gave better results than the other strong forces.

From the above we conclude that the tensor forces used are too weak and that to obtain a reasonable fit to the cross section shape one must use an unphysically weak central force, leading finally to a substantial underestimate of the cross section. Perhaps it is worth noting that calculations with a similar force[13] underestimated the cross section for the $^{14}N(p,n)^{14}O$ (g.s.) cross section at $E_p = 12.2$ MeV by almost a factor of five. It appears that a 1.4 fm range central force is somewhat superior to a 1.0 fm range force and that there is no compelling reason to use exchange mixtures such as HJ + G which are more complex than the Serber mixture.

The following procedure was used to extract empirical estimates of the tensor force. We began with the sum of the central force S (a Serber force with a range of 1.415 fm), the OPEP tensor force and the spin-orbit force for $R_{co} = 0.49$ fm. The strength of the tensor force was then adjusted to obtain the best overall agreement with the shape of the experimental angular distribution. It was found that $1.25 \times V_\tau^{ten}$ (OPEP) was the best choice, with an uncertainty of perhaps ±10% at the two lower energies and ±15% at the two higher energies. Having obtained the best shape in the context of this model, the entire angular distribution was normalized by eye to produce the best overall fit in magnitude with emphasis on reproducing the forward angle data. If the normalization factor is f, this is equivalent to multiplying all the interaction strengths by $\sqrt{f}$. The final fits are shown in Fig. 4 and values of f and V_τ^{ten} are given in Table VI. Since in most cases f > 1, the effective central force used in the calculations is stronger than that listed under S in Table III and is in better agreement with the empirical results for this force as summarized in the force SMA and Ref. 64. At the higher energies f ≃ 1 and V^{cent} remains

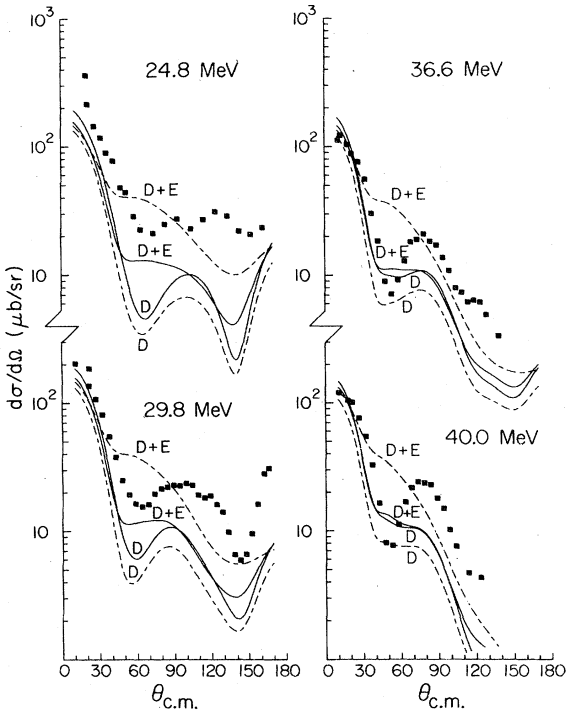

Fig. 12. Differential cross sections for exciting the 2.31 MeV state calculated with central plus tensor forces. The dashed curves show the results for a strong central force, HJ + HJT (R_{CO} = 0.49 fm) while the solid curves show those for a weak central force, S + OPEP. For other details see the caption of Fig. 11.

relatively weak, possibly because of compromises made to achieve the best average shape at all energies.

The normalization technique used here also corresponds to increasing the spin-orbit force from its initial value. However, the effects of this force are sufficiently small (see Fig. 8) and its value sufficiently uncertain that the errors introduced are considerably less than other uncertainties in the analysis.

While the fits we have obtained are reasonably satisfactory at 24.8 and 29.8 MeV, we could not reproduce the prominent peak which appears near $\theta_{c.m.} = 80°$ at the higher bombarding energies. Furthermore, it seems unlikely (see Figs. 8, 9) that reasonable modifications of the input parameters could substantially improve the fits to the high energy data.

In order to understand the nature of the discrepancy between theory and experiment, we have compared the variation with energy of the experimental and DWA cross sections on a plot vs momentum transfer q in Fig. 13. The DWA predictions for S + 1.25 × OPEP + LS forces are nearly independent of energy for $q < 1.9$ fm^{-1} while the experimental cross sections have a smooth but rather marked energy dependence. The data at 36.6 and 40 MeV are rather similar to recent results at 122 MeV,[71] which have a back angle peak of the same magnitude near 1.4 fm.$^{-1}$ It has also proven difficult to obtain accurate fits of the 122 MeV data. If one takes the point of view that it is the apparently stable backward peak that should be fitted, one obtains values of f which are nearly independent of energy (see Fig. 14).

It is not clear why DWA calculations do not accurately reproduce the data. A possibility is that the form of the force chosen is too simple, but a calculation with a rather complicated G-matrix interaction,[62] results shown in Fig. 10, does not describe the data better, nor does a calculation, not shown, with a recent empirical central interaction.[64] Another possibility is that multistep processes contribute to this rather small cross section. Such processes cannot be dominant, since the spin flip fraction is $\gtrsim 0.8$ at 32.0 MeV,[72] but rather small interfering amplitudes might produce the observed dip near $q = 1.2$ fm.$^{-1}$ Indeed, calculations at lower energies[14] show that channel coupling produces non-negligible effects for the transition to the 2.31 MeV state. Cross sections for all the relevant channels are now available[12] and may permit a rigorous test of the coupled channel calculation. Finally, it is possible that the wave functions are inadequate, the results for the empirically derived wave functions[61] differing greatly from those for the Cohen-Kurath wave functions.[52]

E. Results and discussion-3.95 and 7.03 MeV states

Calculations were performed for the other states in ^{14}N whose dominant components are from the 1p shell, namely, the second excited state at 3.95 MeV (1^+, T = 0) and the ninth excited state at 7.03 MeV (2^+, T = 0). It was found that only the J = 2 amplitude is important for the 3.95 MeV state, J = 0 contributing less than 1% and J = 1 about 10% to the cross section at 29.8 MeV. For the 7.03 state the J = 1 amplitude is largest, J = 2 contributing 20% and J = 3 less than 1% of the cross section at 29.8 MeV. Because the code DWBA 70 is written in the helicity notation and sums amplitudes for all values of L and S corresponding to a given J, it was not possible to dissect an amplitude for a particular J. One expects, however, that the (L,S,J,T) = (2,0,2,0) part of the amplitude will be enhanced by collective effects and that other parts will be less affected. Atkinson and Madsen[49] have shown that for N = Z nuclei the enhancement factor ϵ_{pp} for inelastic scattering is approximately equal to that for electromagnetic transitions, ϵ_{EM}. The final cross section was then obtained by summing cross sections for various J, with the J = 2 cross section multiplied by ϵ_{EM}. This involves the additional assumption that the (2,1,2,0) amplitude is much less than (2,0,2,0).

Values of ϵ_{EM} were obtained by comparing the experimental B(E2) values for transitions from the ground state (3.4 ± 0.3 e^{2}fm^4 and 3.5 ± 0.3 e^{2}fm^4 from Refs. 61 and 73, respectively, for the 3.95 MeV state; 2.4 e^{2}fm^4 ± 27% from Ref. 4 for the 7.03 MeV state) with the values we calculated from the CK wave functions (1.71 e^{2}fm^4 and 0.796 e^{2}fm^4, respectively). The enhancement factors are then 2.0 (3.95 MeV) and 3.0 (7.03 MeV). There is some uncertainty in these numbers, especially for the 3.95 MeV state, where the recent B(E2)'s from Refs. 61 and 73 are almost a factor of two smaller than earlier results.[4]

The SMA central force was used in the calculation, as this force has been shown to correctly predict the magnitude of the cross sections for strongly excited states in this mass region.[7,64] The results are shown in Figs. 5 and 6. The magnitudes of the cross sections are approximately correct, although the shapes are only qualitatively reproduced. This discrepancy can perhaps be ascribed to the crudity of the effective charge approximation or to the neglect of the imaginary part of the two body interaction.

VII. SUMMARY

Cross sections for the ^{14}N(p,p')^{14}N reaction leading to the 0.0, 2.31 and 3.95 MeV states of ^{14}N have been

Table VI. Empirical values of the tensor force.

Determination	V_τ^{ten} [a]	f [b]	μ(fm) [c]	μ'(fm) [d]	$J_2(T = 1)$ (MeV fm^5)
$^{14}N(p,p')^{14}N$ (2.31 MeV, 0^+, 1) [e]					
E_p = 24.8	19.2	1.95	0.816		7000 [f]
29.8	16.3	1.40	0.816		5900 [f]
36.0	13.3	0.93	0.816		4800 [f]
40.0	15.0	1.18	0.816		5400 [f]
$^{14}N(p,p')^{14}N$ (2.31 MeV, 0^+, 1) [g]					
E_p = 18 MeV	5.5		1.408	0.5	5000
21	5.6		1.408	0.5	5100
23	5.0		1.408	0.5	4600
26	4.2		1.408	0.5	3800
$^{14}N(p,p')^{14}N$ (2.31 MeV, 0^+, 1)					
E_p = 24.8 MeV [h]	3.9		1.401	0.5	3500
29.8 MeV [i]	14.6		0.816		5300 [j]
$^{14}C(p,n)^{14}N$ (g.s.) [k]					
E_p = 10.4 MeV	5.4		1.401	0.25	5300
12.7	5.1		1.401	0.25	5000
13.3	5.1		1.401	0.25	5000
18.3	3.9		1.401	0.25	3800
$^{12}C(p,p')^{12}C$ (15.1 MeV, 1^+, 1) [l]					
E_p = 45.5 MeV	2.35				2400 [j]

[a] Units are MeV fm^{-2} for the $r^2 \times$ Yukawa potentials and MeV for the regularized OPEP potentials. See footnotes c and d.

[b] This is the normalization factor f described in the text.

[c] When only a range μ is given the potential is of form $V_\tau^{ten}\, r^2 \frac{e^{-r/\mu}}{r/\mu}$.

[d] When ranges μ and μ' are given the potential is of form $V_\tau^{ten}[f(\mu) - (\frac{\mu}{\mu'})^3 f(\mu')]$ where $f(\mu) = [1 + 3\frac{\mu}{r} + 3(\frac{\mu}{r})^2]\frac{e^{-r/\mu}}{r/\mu}$.

[e] Present work.

[f] Analysis includes the exchange amplitude and a spin-orbit force.

[g] Lutz et al., Ref. 15.

[h] Ref. 17.

[i] Ref. 7.

[j] Analysis includes the exchange amplitude.

[k] Ref. 11.

[l] Ref. 50. Tensor force has OPEP form.

measured at bombarding energies of 29.8, 36.6 and 40.0 MeV. In addition, at 29.8 MeV, angular distributions were obtained for the excited states lying below 8.6 MeV.

A systematic optical model analysis was made using the elastic scattering data from the present experiment and that of Crawley et al.[17] at 24.8 MeV. As is common with light nuclei, it was not possible to accurately reproduce the cross section beyond the second diffraction minimum. To determine whether this difficulty might be caused by the strong contributions of the Thomas spin-orbit force in

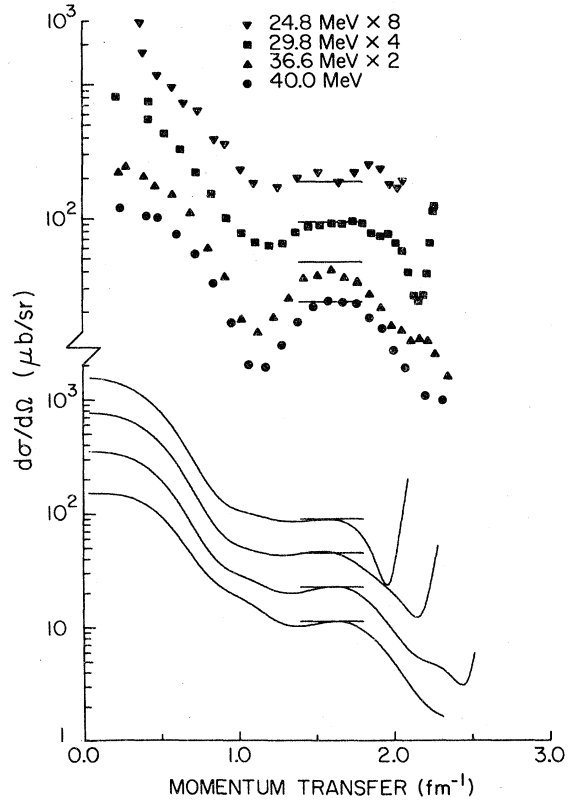

Fig. 13. Differential cross sections for inelastic scattering to the 2.31 MeV state, plotted as a function of the linear momentum transfer q. The data at 24.8 MeV are from Ref. 17. The cross sections have been multiplied by the factor shown for display purposes. All theoretical cross sections in the lower part of the figure were calculated using the force (S + 1.25 × OPEP + LS). The short horizontal lines represent a cross section of 1.12×10^{-2} mb/sr (2.35×10^{-2} mb/sr) for the theoretical (experimental) cross sections.

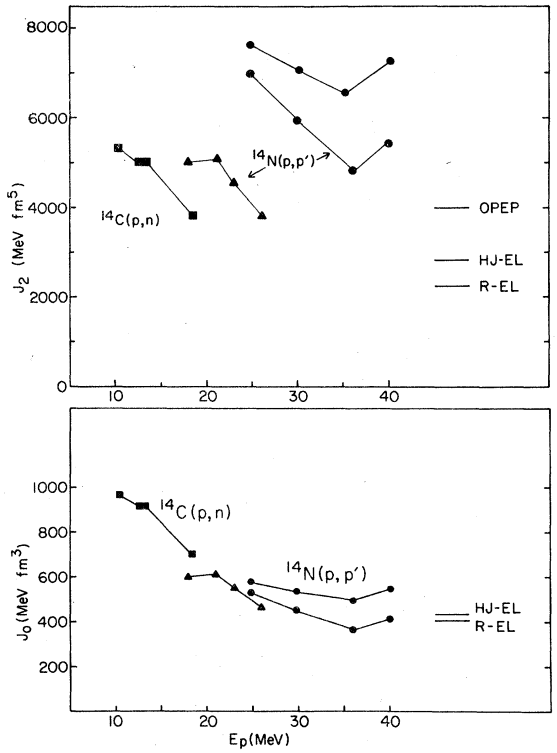

Fig. 14. Values of J_0 and J_2 for the tensor force v_τ^{ten}, obtained from the $1^+0 \leftrightarrow 0^+1$ transition in the mass–14 system. The points ■, ▲ and ● are from Ref. 11, Ref. 15 and the present work respectively. The upper points at 24.8, 29.8, 36.6 and 40.0 MeV are obtained if one normalizes the curves of Fig. 4 at the backward angle peak near q = 1.5 fm^{-1}, and the lower points when the curves are normalized as shown. The horizontal lines are values J_n for the OPEP interactions and for the two interactions from Ref. 62 given in Table IV.

the nuclear interior, we tried a modified[39] spin-orbit potential which was not singular at the origin. The fits were not substantially improved. The real potential is well represented by $V_R = 63.8 - 0.50$ E MeV; the values of the potential obtained are shown in Table II and the approximate variation with energy of the other potential strengths is given in Fig. 7 and Eq. (2).

The cross sections for excitation of the 2.31 MeV state were compared with microscopic model DWA calculations including the contribution from the knock-on exchange amplitude. The wave functions were calculated from the (8–16)2BME two body matrix elements of Cohen and Kurath.[52] Central, tensor and spin orbit effective interactions were employed; it was found that the tensor force dominates the forward angle cross section. The strengths of the potentials were then adjusted to fit the cross sections and the values of V_τ^{ten} (see Eq. 5) shown in Table VI were extracted. The strengths of V_τ^{ten} obtained are larger than the estimates based on the OPEP or the Hamada-Johnston potential. However, in spite of the fact that the present analysis is the most complete to date, the cross sections at 36.6 and 40.0 MeV are not accurately reproduced.

If one adopts the suggestion of Wong et al.,[11] that the J_2 integral is a reasonable measure of the strength of a tensor interaction, one can also compare our results with interaction strengths obtained using other radial shapes (see Table VI and Fig. 14). The differences between our strengths and the smaller values found in the earlier work are probably due, at least in part, to our inclusion of the effects of exchange and of the spin orbit force, both of which depress the cross section and lead to larger values of V_τ^{ten}. The discrepancy in the case of the ^{12}C(p,p')^{12}C (1^+, T = 1, E_x = 15.1 MeV) reaction is particularly large and may be due to the fact that the central force used in the calculation was greatly simplified ($V_{00} = V_{10} = V_{01} = 0$), as were the wave functions.

For the transition to the 2.31 state, calculations show that the cross section is approximately proportional to J_0 rather than J_2, at least for the $r^2 \times$ Yukawa tensor interaction. This, of course, implies that large values of momentum transfer are important.[12] Values of J_0 from various empirical interactions are also shown in Fig. 14.

The states at 3.95 MeV (1^+, T = 0) and 7.03 MeV (2^+, T = 0) are presumably dominated by lp shell orbitals[53] and hence are reasonably well described by the Cohen-Kurath wave functions. Calculations for these states were made taking into account collective effects using the effective charge approximation of Atkinson and Madsen.[49] The magnitudes of the predicted cross

sections are reasonable, although the shapes are only qualitatively correct.

ACKNOWLEDGMENTS

We wish to thank R. Schaeffer for making available the code DWBA 70 and for much useful advice. The assistance of D.C. Larson with data acquisition and the theoretical analysis is gratefully acknowledged. We had helpful discussions with G. Bertsch, P. Hauge, H. McManus, F. Petrovich, and B.H. Wildenthal.

This material is based upon work supported by the National Science Foundation under Grant No. Phy-7822696.

---

*Present address: E552 Medical Science Bdlg., University of Cincinnati Medical Center, Cincinnati, Ohio 45267.

[1]B. Janocovici and I. Talmi, Phys. Rev. 95, 289 (1954).
[2]J.P. Elliott, Phil. Mag. 1, 503 (1956).
[3]W.M. Visscher and R.A. Ferrell, Phys. Rev. 107, 781 (1957).
[4]F. Ajzenberg-Selove, Nucl. Phys. A268, 1 (1976).
[5]D.R. Inglis, Rev. Mod. Phys. 25, 390 (1953).
[6]H.J. Rose, O. Hausser and E.K. Warburton, Rev. Mod. Phys. 40, 591 (1968).
[7]S.M. Austin in The Two Body Force in Nuclei, edited by S.M. Austin and G.M. Crawley (Plenum Press, New York 1972), p. 285.
[8]C.A. Levinson and M.K. Banerjee, Ann. Phys. 2, 471 (1957).
[9]C. Wong, J.D. Anderson, J. McClure, B. Pohl, V.A. Madsen and F. Schmittroth, Phys. Rev. 160, 769 (1967).
[10]V.A. Madsen, V.R. Brown, F. Becchetti and G.W. Greenlees, Phys. Rev. Lett. 26 454 (1971).
[11]C. Wong, J.D. Anderson, V.A. Madsen, F.A. Schmittroth and M.J. Stomp, Phys. Rev. C 3, 1904 (1971).
[12]T.N. Taddeucci, R.K. Doering, L.C. Dennis, A. Galonsky and S.M. Austin, Bull. Am. Phys. Soc. 24, 594 (1979); R.R. Doering, T.N. Taddeucci, A. Galonsky and D.M. Patterson, Phys. Rev. C20, 1627 (1979).
[13]W.G. Love, L.J. Parish and A. Richter, Phys. Lett. 31B, 167 (1970).
[14]L.F. Hansen, S.M. Grimes, J.L. Kammerdiener and V.A. Madsen, Phys. Rev. C 8, 2072 (1973).
[15]T.H. Curtis, H.F. Lutz, D.W. Heikkinen and W. Bartolini, Nucl. Phys. A165, 19 (1971); H.F. Lutz, D.W. Heikkinen and W. Bartolini, Nucl. Phys. A198, 257 (1972).
[16]J.-L. Escudie, A. Tarrats and J. Raynal, in Polarization Phenomena in Nuclear Reactions, edited by H.H. Barschall and W. Haeberli (University of Wisconsin Press, Madison 1970), p. 705.
[17]G.M. Crawley, S.M. Austin, W. Benenson, V.A. Madsen, F.A. Schmittroth and M.J. Stomp, Phys. Lett. 32B, 92 (1970).
[18]V.V. Bobyr', L. Ya. Grona and V.I. Strizhak, Zh. Eksp. Teor. Fiz. 41, 24 (1961) [transl: Sov. Phys.-JETP 14, 18 (1962)].
[19]G.F. Trentelman and E. Kashy, Nucl. Instrum. Methods 82, 304 (1970).
[20]W.L. Pickles, Ph.D. Thesis, Michigan State University (1970), unpublished.
[21]H.W. Laumer, Ph.D. Thesis, Michigan State University (1971), unpublished.
[22]D.L. Bayer, MSUCL-34, Michigan State University Cyclotron Laboratory (1971), unpublished.
[23]E.A. Silverstein, Nucl. Instrum. Methods 4, 53 (1959).
[24]T.A. Cahill, F.P. Brady, S. Corbett, W. Hammontree, K. Isaacs and E. Young, Nucl. Instrum. Methods 87, 151 (1970).
[25]D.R. Maxson, R.K. Jolly and K.C. Knox, Nucl. Instrum. Methods 62, 276 (1968).
[26]M.Q. Makino, C.N. Waddell and R.M. Eisberg, Nucl. Phys. 50, 145 (1969).
[27]T.J. Gooding, Nucl. Phys. 12, 241 (1959).
[28]K.M. Thompson, C.R. Gruhn and J. Frink, Phys. Lett. 24B, 503 (1967).
[29]M. Makino, R. Eisberg, K. Richie, R. Carlson and C. Waddell, Nucl. Instrum. Methods 80, 299 (1970).
[30]J.J. Kraushaar, R.A. Ristinen and R. Smythe, Phys. Lett. 25B, 13 (1967).
[31]T.R. King, J.J. Kraushaar, R.A. Ristinen, R. Smythe and D.M. Stupin, Nucl. Instrum. Methods 88, 17 (1970).
[32]C.R. Gruhn, private communication.
[33]J.T. Routti and S.G. Prussin, Nucl. Instrum. Methods 72, 125 (1969).
[34]An optical model search code written by F.G. Perey and modified by R.M. Haybron at Oak Ridge National Laboratory.
[35]J.L. Snelgrove and E. Kashy, Phys. Rev. 187, 1259 (1969).
[36]W.T.H. van Oers and J.M. Cameron, Phys. Rev. 184, 1061 (1969).
[37]G.M. Crawley, private communication.
[38]H.S. Sandhu, Nucl. Phys. A146, 163 (1970).
[39]B.A. Watson, P.P. Singh and R.E. Segel, Phys. Rev. 182, 977 (1969).
[40]C.C. Kim, S.M. Bunch, D.W. Devins and H.H. Forster, Nucl. Phys. 58, 32 (1964).
[41]F.G. Perey, Phys. Rev. 131, 745 (1963).
[42]M.P. Fricke, E.E. Gross, B.J. Morton and A. Zucker, Phys. Rev. 156, 1207 (1967).
[43]E.E. Gross, R.H. Bassel, L.N. Blumberg, B.J. Morton, A. van der Woude and A. Zucker, Nucl. Phys. A102, 673 (1967).
[44]G.R. Satchler, Nucl. Phys. 77, 481 (1966); V.A. Madsen, Nucl. Phys. 80, 177 (1966); N.K. Glendenning and M. Veneroni, Phys. Rev. 144, 839 (1966).
[45]W.G. Love and G.R. Satchler, Nucl. Phys. A159, 1 (1970).
[46]F. Petrovich, H. McManus, V.A. Madsen and J. Atkinson, Phys. Rev. Lett. 22, 895 (1969).
[47]D. Agassi and R. Schaeffer, Phys. Lett. 26B, 703 (1968); and R. Schaeffer, Nucl. Phys. A132, 186 (1969).
[48]K.A. Amos, V.A. Madsen and I.E. McCarthy, Nucl. Phys. A94, 103 (1967); K.A. Amos, Nucl. Phys. A103, 657 (1967); and H.V. Geramb and K.A. Amos, Nucl. Phys. A163, 337 (1971).
[49]J. Atkinson and V.A. Madsen, Phys. Rev. C 1, 1377 (1970).
[50]W.G. Love and L.J. Parish, Nucl. Phys. A157, 625 (1970).
[51]R. Schaeffer and J. Raynal, unpublished.
[52]S. Cohen and D. Kurath, Nucl. Phys. 73, 1 (1965).
[53]N.F. Mangelson, B.G. Harvey and N.K. Glendenning, Nucl. Phys. A117, 161 (1968).
[54]F. Ajzenberg-Selove, Nucl. Phys. A320, 1 (1979).
[55]W.W. True, Phys. Rev. 130, 1530 (1963).
[56]B.S. Reehal and B.H. Wildenthal, unpublished.
[57]J.B. French, E.C. Halbert, J.B. McGrory and S.S.M.

Wong in Advances in Nuclear Physics, Vol. III, edited by M. Baranger and E. Vogt (Plenum Press, New York 1969), p. 193.
[58]D. Larson, S.M. Austin and B.H. Wildenthal, Phys. Lett. 42B, 153 (1972); Phys. Rev. 11, 1638 (1975).
[59]G.R. Bishop, H. Bernheim, P. Kossanyi-Demay, Nucl. Phys. 54, 353 (1964).
[60]E.B. Dally, M.G. Croissiaux and B. Schweitz, Phys. Rev. C2, 2057 (1970).
[61]N. Ensslin, W. Bertozzi, S. Kowalski, C.P. Sargent, W. Turchinetz, C.F. Williamson, S.P. Fivozinsky, J.W. Lightbody, Jr. and S. Penner, Phys. Rev. C9, 1705 (1974); W.G. Love, private communication.
[62]G. Bertsch, J. Borysowicz, H. McManus, and W.G. Love, Nucl. Phys. A284, 399 (1977).
[63]W.G. Love, Phys. Lett. 35B, 371 (1971); Nucl. Phys. A192, 49 (1972).
[64]S.M. Austin, Telluride Conference on the (p,n) Reaction and the Nucleon-Nucleon Force, Telluride, Colo., 1979 (unpublished).
[65]W.G. Love, Telluride Conference on the (p,n) Reaction and the Nucleon-Nucleon Force, Telluride, Colo., 1979 (unpublished).
[66]R. Schaeffer, private communication.
[67]L.W. Owen and G.R. Satchler, Phys. Rev. Lett. 25, 1720 (1970).
[68]J.M. Blatt and J.D. Jackson, Phys. Rev. 76, 18 (1949).
[69]T. Hamada and I.D. Johnston, Nucl. Phys. 34, 382 (1962).
[70]G.W. Greenlees, G.J. Pyle and Y.C. Tang, Phys. Rev. 171, 1115 (1968).
[71]J.R. Comfort, S.M. Austin, P. Debevec, G. Moake, R. Findlay and W.G. Love (unpublished).
[72]J.M. Moss, p. 78 in Proceedings of the INS International Symposium on Nuclear Direct Reaction Mechanism, edited by M. Tanifuji and K. Yazaki (Institute for Nuclear Study, Tokyo, 1979). Data are for $\theta<30^{\circ}$ only.
[73]M. Bister, A. Anttila and J. Keinonen, Phys. Rev. C 16, 1303 (1977).